When energy isn't enough: Understanding structural failures in VQE

Ganga Singh Manchanda*
Quantum Optics and Laser Science Group, The Blackett Laboratory, Imperial College, Prince Consort Rd., London, SW7 2BZ, United Kingdom
(Dated: August 15, 2025)

The variational quantum eigensolver (VQE) relies solely on energy minimisation to approximate ground states. We demonstrate that, for a weak ansatz, this may be insufficient by outlining instances where closeness in energy does not correspond to closeness in state. Studying the transverse field Ising model, we find that a Trotterised ansatz successfully reproduces the energy spectrum of the true ground state along with key observables. A hardware-efficient ansatz on the other hand, fails to reproduce those same key observables even when it matches the energy spectrum. We propose three potential sources of failure in the VQE sequence—deep-local minima, non-linear error amplification, and resolution ambiguity—and examine how they contribute to this result. These failure modes are notable because they occur even when energy is successfully minimised, unlike local minima, barren plateaus, and other challenges discussed in the literature. They arise not from poor optimisation, but rather from the structure of the variational landscape (inherent to ansatz choice) and are amplified near quantum phase transitions where the spectral gap vanishes. Our results highlight the need for careful ansatz design and more comprehensive benchmarking, beyond energy minimisation, if VQE is to be a reliable tool in quantum chemistry and quantum many-body simulation.

I. INTRODUCTION

The variational quantum eigensolver (VQE) is a leading candidate for near-term quantum simulation, promising (as yet unproven) exponential advantage over classical methods [1]. Its potential impact in quantum chemistry and condensed matter physics is considerable [2, 3] and yet many argue against generic exponential quantum advantage citing concerns over fault tolerance, classical competition, and ansatz design [4]. The latter point can be quite subtle and we contribute to the discourse by identifying and analysing structural failures that can occur with weaker ansätze.

VQE approximates the ground state of a Hamiltonian via minimisation of the energy expectation value. We demonstrate that energy minimisation alone can be insufficient to reproduce key observables—such as entanglement entropy, entanglement spectrum, or fidelity—of the variational state of a system through violation of a key (often implicit) assumption, that closeness in energy corresponds to closeness in state. VQE, being grounded in energy minimisation, is blind to these failures such that great caution must be taken. These discrepancies undermine the reliability of VQE for applications where computing these observables is essential.

Most documented challenges in VQE (barren plateaus [5], local minima [6, 7], expressivity-trainability trade-off [8, 9], and so on) are characterised by a failure to minimise energy. By contrast, we study instances where energy is successfully minimised yet the variational state continues to misrepresent key features of the true ground state. These failures are rooted in the structure of the variational landscape, not in poor optimisation, and become especially pronounced for a class of Hamiltonians with small spectral gaps, such as those near quantum phase transitions. Such failures have been hinted at in the context of quantum chemistry [10].

We propose three mechanisms of failure to explain our findings. First is *deep-local minima*: where low energy states of incorrect structure trap the optimiser. Second is *non-linear error amplification*: where small energy deviations (like those due to deep-local minima) lead to disproportionately large errors in certain observables. Third and last is *resolution ambiguity*: where small spectral gaps can lead to indistinguishable low energy states.

When investigating a novel physical system, little is known about the ground state *a priori*. If the energy is known, then it is used as a benchmark to validate the variational state. This paper highlights the need for comprehensive benchmarking beyond energy and encourages the use of problem-oriented ansätze to avoid the pitfalls described.

The structure of the paper is as follows. In Section II we describe the methods of our investigation, outlining the VQE algorithm and the two ansätze we study: Trotterised and hardware-efficient. In Section III, we present simulations of the transverse field Ising model (TFIM) in 1D and 2D along with instances of structural failure. In Section IV we propose the mechanisms of failure and explain how they support the TFIM results. Finally, in Section V we discuss the broader implications of these findings for the future of VQE and suggest potential approaches for improving the algorithm's reliability.

* ganga@manchanda.co.uk

II. METHODS

We begin by outlining the VQE algorithm and the two types of ansatz we study: Trotterised and hardware-efficient. These are the methods by which we simulate the TFIM Hamiltonian [11, 12]:

$$\hat{H} = -\sum_{\langle ij \rangle}^{n} \hat{\sigma}_i^z \hat{\sigma}_j^z - h \sum_{i}^{n} \hat{\sigma}_i^x. \tag{1}$$

A. Variational quantum eigensolver

The foundation of VQE is the variational principle: Any arbitrary state $|\psi\rangle \in \mathcal{H}$ must satisfy $\langle\psi| \hat{H} |\psi\rangle \geq E_0$. For a Hamiltonian expressed as a Pauli string, a quantum computer can readily evaluate the energy expectation value such that to estimate its ground state [1]:

1. Prepare an ansatz state $|\psi(\boldsymbol{\theta})\rangle = U(\boldsymbol{\theta}) |0\rangle^{\otimes n}$ based on some parameter vector $\boldsymbol{\theta}$.
2. Evaluate the energy expectation value of this state, $E(\boldsymbol{\theta}) = \langle\psi(\boldsymbol{\theta})| \hat{H} |\psi(\boldsymbol{\theta})\rangle$.
3. Use gradient descent to minimise $E(\boldsymbol{\theta})$ by varying the parameter $\boldsymbol{\theta}$.

Once gradient descent reaches a (hopefully global) minimum, the parameter must specify an upper bound on the ground state energy, $E(\boldsymbol{\theta}) \geq E_0$. A key assumption made in VQE is that closeness in energy, $E(\boldsymbol{\theta}) \approx E_0$, implies closeness in state, $|\psi(\boldsymbol{\theta})\rangle \approx |\psi_0\rangle$, but we shall show that this is not always the case.

We perform our VQE in Pennylane, with an ADAM optimiser converging at a cost difference of 10^{-8}. As we shall repeat the process across a range of values for the transverse field, h, we use a "warm start" approach where the optimised parameter for h_i, is the starting parameter of the ansatz for h_{i+1} [13]. Given a sufficiently small gap between adjacent h values, we expect a small gap between $\boldsymbol{\theta}_i$ and $\boldsymbol{\theta}_{i+1}$ such that this strategy speeds up the optimisation process.

B. Trotterised ansatz

In the balancing act between expressiveness and trainability, our compromise lies with an ansatz which mirrors the topology of the 1D TFIM by generating entanglement only between neighbouring qubits. In doing so we narrow down the variational landscape from the arbitrary Hilbert space to the space of physical states. With this in mind, we take inspiration from quantum approximate optimisation algorithm [14, 15] and consider a Trotterised evolution, $|\psi(\boldsymbol{\theta})\rangle = e^{-i\hat{H}\boldsymbol{\theta}} |+\rangle^{\otimes n}$, of a generic mixed state, $|+\rangle^{\otimes n}$, that should have some overlap with the ground state. Naturally, (1) splits into non-commuting H_{ZZ} and H_X terms which can be reproduced by the sequences CNOT $\circ$ R$_Z$ $\circ$ CNOT and R$_X$ respectively. Applying these gates (as drawn in FIG. 1) to every qubit p times sufficiently approximates the unitary.

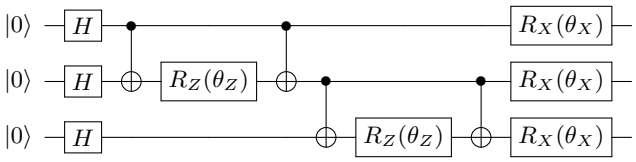

FIG. 1: Circuit diagram of the Trotterised ansatz initialised from $|0\rangle$ for $n = 3$ and $p = 1$. θ_Z and θ_X may vary between layers. The ansatz used in practice typically composes several of these layers, $p > 1$.

In 2D, the summation in the Hamiltonian extends to nearest neighbour interactions and the ansatz is adapted accordingly.

C. Hardware-efficient ansatz

Next we consider a generic hardware-efficient ansatz, designed to be broadly applicable across different quantum systems. Each layer applies R$_X$ $\circ$ R$_Y$ to every qubit followed by an entangling CZ gate between neighbours (as drawn in FIG. 2)

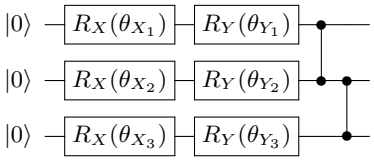

FIG. 2: Circuit diagram of the hardware-efficient ansatz initialised from $|0\rangle$ for $n = 3$ and $p = 1$. θ_{X_i} and θ_{Y_i} may vary between layers. The ansatz used in practice typically composes several of these layers, $p > 1$.

Comparing to the Trotterised ansatz, we gain versatility at the expense of expressivity (at low circuit depth). Entanglement is generated at a slower rate such that to represent a highly entangled state takes more layers than the Trotterised ansatz would need.

III. TFIM SIMULATIONS

In this section we simulate the 1D and 2D TFIM, focussing on a few key observables [16–18]. First is the von Neumann entanglement entropy:

$$S = -\mathrm{Tr}\left(\rho_{\frac{1}{2}} \log_2 \rho_{\frac{1}{2}}\right), \tag{2}$$

where $\rho_{\frac{1}{2}} = \mathrm{Tr}_{\frac{1}{2}} |\psi(\boldsymbol{\theta})\rangle \langle\psi(\boldsymbol{\theta})|$ is the half-chain reduced density matrix. Second is the entanglement spectrum:

$\{\xi_i\}$ (the set of ordered eigenvalues of $\rho_{\frac{1}{2}}$), and third is the fidelity between the variational state and exact ground state:

$$F = |\langle\psi_0|\psi(\boldsymbol{\theta})\rangle|^2. \tag{3}$$

A. 1D

In the open boundary 1D TFIM, we expect the system to exhibit a quantum phase transition (QPT) at $h = 1$ from an ordered ferromagnetic phase to a disordered paramagnetic phase.

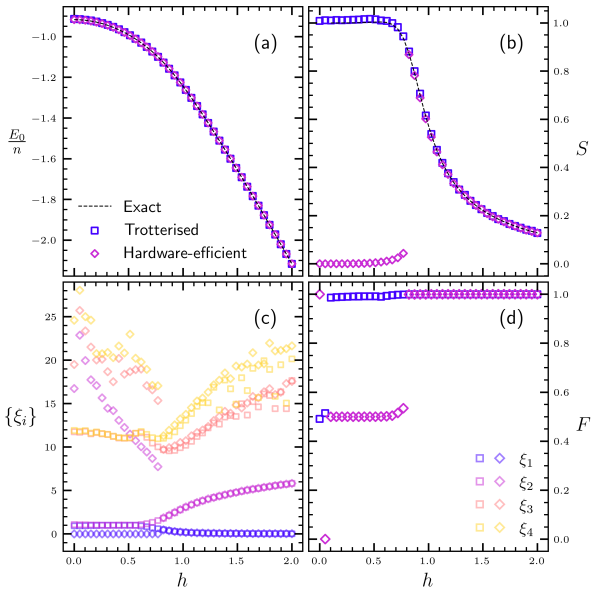

FIG. 3: 1D TFIM for $n = 12$ and $p = 12$. (a) $h - \frac{E_0}{n}$ energy plot and (b) $h - S$ von Neumann half-chain entanglement entropy plot comparing exact diagonalisation, Trotterised ansatz, and hardware-efficient ansatz. (c) $h - \xi_i$ entanglement spectrum plot of the four largest eigenvalues comparing Trotterised ansatz and hardware-efficient ansatz. (d) $h - F$ fidelity plot comparing Trotterised ansatz and hardware-efficient ansatz.

FIG. 3(a) demonstrates that VQE accurately reproduces the ground state energy across a range of h for both the Trotterised and hardware-efficient ansätze. Typically this would be sufficient to verify that both ansätze lead to a successful approximation of the ground state, entropy however tells a different story.

At $h = 0$, the ground state consists of two degenerate configurations forming a maximal entropy GHZ or "cat" state:

$$|\psi_0\rangle = \frac{1}{\sqrt{2}}\left(|0\rangle^{\otimes n} + |1\rangle^{\otimes n}\right). \tag{4}$$

As h increases from 0, the degeneracy is lifted and entanglement decreases as we approach the QPT at $h = 1$. Past the QPT, as $h \to \infty$, the system approaches a product state and the entanglement entropy vanishes [19].

From FIG. 3(b), the Trotterised ansatz captures these features exactly [20] (subject to finite-size effects [21, 22]), while the hardware-efficient ansatz completely misses the GHZ state. The variational state obtained via this ansatz, while close in energy, differs significantly in entanglement structure.

To examine finer structure, we consider the entanglement spectrum in FIG. 3(c). The Trotterised ansatz leads to a gapless spectrum for $h < 1$ and a gapped spectrum for $h > 1$ in line with expectations [23]. Past the QPT, higher levels (ξ_3, ξ_4) fluctuate, indicating increased correlation length and sensitivity to wavefunction errors. On the other hand, the hardware-efficient ansatz fails to exhibit degeneracy near $h = 0$, and the gapless to gapped transition vanishes.

The fidelity, as seen in FIG. 3(d), further supports these conclusions as the Trotterised ansatz reaches $F \approx 1$ across h while the hardware-efficient ansatz achieves this only for $h \gtrsim 1$. As the number of layers is increased, the accuracy of the hardware-efficient ansatz approaches that of the Trotterised ansatz but *a priori* it is impossible to know that these layers are necessary, even when benchmarking against energy.

B. 2D

Extending to 2D, the QPT is shifted to $h \approx 3.044$ [24]. The greater connectivity of the lattice increases entanglement between neighbouring qubits such that a greater layer-to-qubit (p/n) ratio is required to achieve similar expressibility to the 1D case. On the whole, we expect similar features in the entanglement distributions.

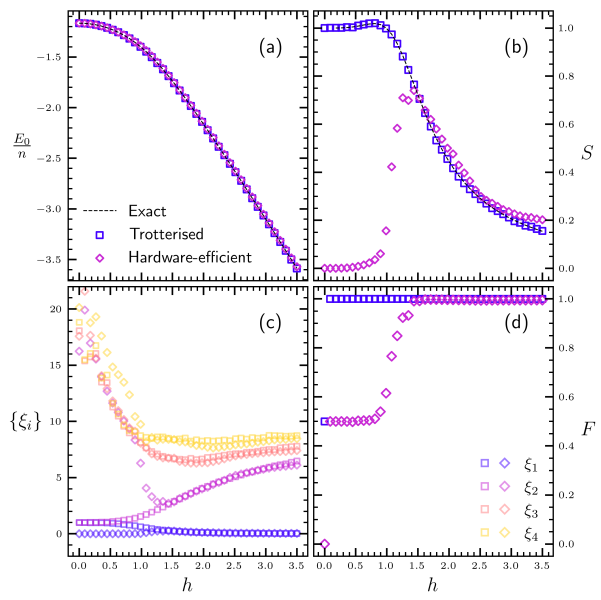

FIG. 4: 2D TFIM for $n = 2 \times 3$ and $p = 9$. (a) $h - \frac{E_0}{n}$ energy plot and (b) $h - S$ von Neumann half-chain entanglement entropy plot comparing exact diagonalisation, Trotterised ansatz, and hardware-efficient ansatz. (c) $h - \xi_i$ entanglement spectrum plot of the four largest eigenvalues comparing Trotterised ansatz and hardware-efficient ansatz. (d) $h - F$ fidelity plot comparing Trotterised ansatz and hardware-efficient ansatz.

Once again the energy distribution, as seen in FIG. 4(a) suggests that VQE has succeeded, and once again something goes awry. FIG. 4(b-d) all match expectations for the Trotterised ansatz [25] and follow the patterns of failure described in the 1D case for the hardware-efficient ansatz.

As the size of the entanglement spectrum scales with the bipartition boundary [26] we expect additional significant eigenvalues in the 2D case, all subject to strong finite-size distortions.

IV. STRUCTURAL FAILURES

To explain the discrepancies of the previous section, we put forward three mechanisms of structural failure. These failures are structural in the sense that they are inherent to the geometry of the variational landscape, rather than our optimisation.

A. Deep-local minima

Though our physical system is described by a Hamiltonian, VQE does not search through the discrete Hamiltonian spectrum. Rather it searches through the continuous variational landscape set out by the ansatz. As such, even though they study the same Hamiltonian, our two ansätze can differ vastly in their geometry with significant consequences for VQE.

As a simple example, consider the two-qubit Hamiltonian in computational basis:

$$H = \mathrm{diag}(0, \Delta, \Delta + \delta, 1), \tag{5}$$

where $0 < \Delta \ll 1$, $\delta > 0$. The Hilbert space possesses a single global minimum, the zero-energy ground state $|00\rangle$. By choosing an ansatz we form the variational landscape from a subset of the Hilbert space, restricting to a space of (hopefully) physical states. Regardless of whether this variational landscape contains $|00\rangle$, it may contain valleys where $E(\theta) \sim \mathcal{O}(E_0)$, but $F \ll 1$. We call these deep-local minima and at a given resolution, they may be indistinguishable from the global minimum. For an ansatz which permits states of the form:

$$|\psi(\lambda)\rangle = \begin{pmatrix} \cos\theta(\lambda) \\ \sin\theta(\lambda)\cos\phi(\lambda) \\ \sin\theta(\lambda)\sin\phi(\lambda) \\ 0 \end{pmatrix}, \tag{6}$$

where $\theta(\lambda) = \frac{\pi}{4} + \frac{\pi}{4}\cos\lambda$ and $\phi(\lambda) = \sin\lambda$, the energy expectation values and ground-state fidelities are

$$E(\lambda) = \sin^2\theta(\lambda)\left[\Delta + \delta\sin^2\phi(\lambda)\right], \tag{7}$$
$$F(\lambda) = \cos^2\theta(\lambda). \tag{8}$$

The global minimum exists at $\lambda = \pi$: $E(\pi) = 0$, $F(\pi) = 1$, but a deep-local minimum also exists at $\lambda = 0$: $E(0) = \Delta$ and $F(0) = 0$ such that for sufficiently small Δ an optimiser could easily confuse the deep-local minimum for the global minimum. It is abundantly clear that this phenomenon is an artefact of the ansatz design.

To visualise the difference between the two ansätze of our investigation, consider the case of the $n = 2$, $h = 1$ TFIM with a layer and qubit independent $\boldsymbol{\theta} = (\theta_1, \theta_2)$. With this system we can map energy and fidelity across the entire variational landscape.

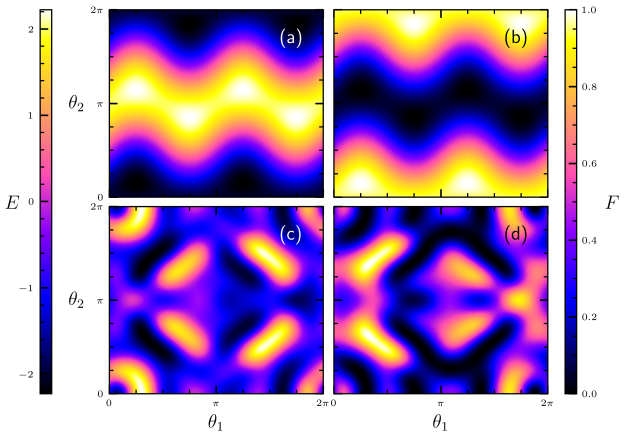

FIG. 5: TFIM for $n = 2$, $p = 1$ (Trotterised ansatz), $p = 3$ (hardware-efficient ansatz), and $\theta_1, \theta_2 \in [0, 2\pi]$. $\theta_1 - \theta_2$ landscape heatmaps for (a) Trotterised ansatz energy, (b) Trotterised ansatz fidelity, (c) hardware-efficient ansatz energy, and (d) hardware-efficient ansatz fidelity. The chosen depths of the ansätze are the minimum required to reach $\delta E = 0.01$.

In FIG. 5(a) and FIG. 5(b), the landscape is simple and the optimiser can easily navigate the trivial transformations between regions where energy is low and fidelity is high, confirming that the Trotterised ansatz is ideal in this context. In FIG. 5(c) and FIG. 5(d), the landscape is much more complicated and rife with disjoint minima such that an optimiser could easily be trapped with a hardware-efficient ansatz.

In the case of the 1D TFIM, it is straightforward to see that the states $|0\rangle^{\otimes n}$ and $|1\rangle^{\otimes n}$ act as deep-local minima with an exact energy match to the GHZ state (4) but only a half match for fidelity, explaining the $F = 0.5$ from FIG. 3(d). Approaching the QPT macroscopic entanglement vanishes, giving the ansatz sufficient expressivity to match the rest of the spectrum. Problem-oriented ansätze avoid these kinds of traps because they can impose relevant symmetries and scaling to restrict the landscape to physical states.

B. Non-linear error amplification

Our discussion of deep-local minima explains how small errors in the energy are introduced, but we are yet to see how that translates to larger errors in our key observables. Let

$$|\psi(\boldsymbol{\theta})\rangle = c_0 |\psi_0\rangle + \sum_{i\geq 1} c_i |\psi_i\rangle , \tag{9}$$

$$1 = |c_0|^2 + \sum_{i\geq 1} |c_i|^2, \tag{10}$$

where c_i are $\boldsymbol{\theta}$-dependent. If VQE minimises energy to within $\delta E = E(\boldsymbol{\theta}) - E_0$, then it is easily shown that:

$$\delta E = \sum_{i\geq 1} |c_i|^2 (E_i - E_0) . \tag{11}$$

The spectral gap defined as $\Delta = E_1 - E_0$, must satisfy $E_i \geq E_0 + \Delta \quad \forall i \geq 1$ such that we can bound the error in energy:

$$\delta E \geq \Delta(1 - F), \tag{12}$$

where we simply reinterpret $|c_0|^2$ as the fidelity, F. The trace distance of the error in the reduced density matrix is $\frac{1}{2}\|\rho(\boldsymbol{\theta}) - \rho_0\|_1 = \sqrt{1-F}$ and with the Fannes-Audenaert inequality [27], we can bound the error in von Neumann entropy:

$$\begin{aligned} |\delta S| \leq & \sqrt{\frac{\delta E}{\Delta}} \log_2(d-1) - \sqrt{\frac{\delta E}{\Delta}} \log_2 \sqrt{\frac{\delta E}{\Delta}} \\ & - \left(1 - \sqrt{\frac{\delta E}{\Delta}}\right) \log_2 \left(1 - \sqrt{\frac{\delta E}{\Delta}}\right), \end{aligned} \tag{13}$$

where d is the dimension of the reduced Hilbert space, $\mathcal{H}_{\frac{1}{2}}$. The inequality saturates at $|\delta S| = \frac{n}{2}$ for maximally distant reduced density matrices, though in practice this is never achieved as the Hilbert space is restricted.

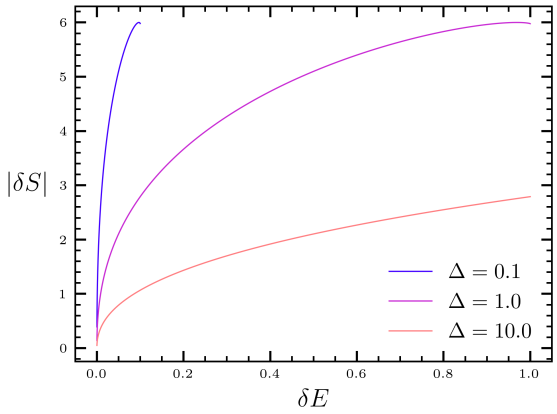

FIG. 6: $|\delta S| - \delta E$ error bound plot for $d = 64$, comparing spectral gaps $\Delta = 0.1$, $\Delta = 1.0$, and $\Delta = 10.0$.

It is clear from FIG. 6 how when VQE results satisfy $\delta E \ll 1$, the error in δS can still be much larger in relative terms such that $\delta S \sim \mathcal{O}(1)$ is possible. As we approach the QPT, the spectral gap vanishes allowing for significant error.

The entanglement spectrum is even more sensitive as if $\rho_{\frac{1}{2}}$ is nearly degenerate, small changes can be amplified into large shifts in the eigenvalues ξ_i. This effect is particularly pronounced for the levels which determine the Schmidt gap, a key signature of quantum phase structure. Other non-linear observables (correlation functions, topological invariants etc) relevant to quantum simulation may present the same sensitivities demonstrated here.

C. Resolution ambiguity

This last point is seemingly trivial, but is quite important in systems with small spectral gaps. It has also played a part in the previous subsections without explicit mention: resolution ambiguity. We can bound the relation between energy error and fidelity error via (12):

$$\delta F \leq \frac{\delta E}{\Delta}. \tag{14}$$

In systems with $\Delta \sim O(1)$, this is reassuring: a small δE bounds a proportionally small δF. In systems with $\Delta \ll O(1)$, particularly near a QPT where $\Delta \to 0$, the bound becomes uninformative as a small δE can be consistent with a large δF.

Resolution ambiguity is more than an isolated failure mode, it underlies the practical impact of deep-local minima and non-linear error amplification. In the presence of deep-local minima, a coarse resolution masks the fact that the optimiser has settled in the wrong basin. In the case of non-linear error amplification, resolution determines how small δE can be driven in practice, and thus how large the resulting errors in non-linear observables may become when Δ is small. In both cases, the collapse of the spectral gap near criticality pushes the system into the ambiguous regime where closeness in energy does not correspond to closeness in state.

In practice, δE is not reduced arbitrarily. The optimisation process halts either when the cutoff is reached or because the inherent noise from finite sampling masks smaller improvements. This leaves us with an effective resolution, δE_{eff}, which defines the smallest energy change the algorithm can reliably detect. When $\delta E_{\text{eff}} \gtrsim \Delta$ distinct states, potentially with very different physical properties, can appear equally optimal within the accessible resolution.

As before, the bound only saturates for arbitrarily distant states, which neither the Trotterised ansatz nor the hardware-efficient ansatz describe. The Trotterised ansatz however still performs much better than the hardware-efficient ansatz as it is problem-oriented such that the Hilbert space is more tightly restricted.

This mechanism plays out clearly in the TFIM. As the field approaches the QPT, the spectral gap collapses and for the finite systems studied here it remains small over a finite window. Within this regime deep-local minima, non-linear error amplification, and resolution ambiguity all contribute to the results we see for the hardware-efficient ansatz.

V. DISCUSSION

Our results show that there exists a class of failure modes in VQE that occur even when the energy spectrum presents as asymptomatic. The severity of these errors depends on both ansatz choice and the Hamiltonian spectral gap. A hardware-efficient ansatz is shown to fail repeatedly where a problem-oriented (Trotterised) ansatz of the same depth succeeds. In the hardware-efficient case, the common assumption that closeness in energy implies closeness in state can fail dramatically, especially in systems with a small spectral gaps or highly entangled structures. The implications of this extends beyond the immediate context of the TFIM.

A central ambition of near-term quantum simulation is to extract physically meaningful observables. Our findings indicate that, the validity of such observables cannot be inferred from energy alone, challenging the notion that variational methods can serve as a general-purpose "black box" for state preparation. Existing estimates for required circuit depth or measurement budget are often based on the energy resolution of VQE such that as we violate the key assumption discussed, these estimates may also break down resulting in a shift of the practical trade-off made during ansatz design.

Current primary performance indicators emphasise an energy benchmark, but as demonstrated this is insufficient. As further observables are not known *a priori* to benchmark against we must rely on inferences from the Hamiltonian to ensure the success of VQE (aside from blindly increasing circuit depth). These inferences come in the form of symmetries, scaling expectations, topological considerations, and so on and they may be implemented in the ansatz, the cost function, or the benchmark. Ansatz implementation is simply moving to a problem-oriented ansatz like the Trotterised one we use. Cost function augmentation is adding a penalisation for states which do not satisfy the symmetries of the Hamiltonian. With cost function augmentation, the complexities of the state are dealt with by classical computation rather than quantum computation which is ideal when dealing with noisy systems. More comprehensive benchmarking against the inferences signal when VQE has experienced failure like we describe in this paper.

These changes may help in the short term. In the longer term, as fault tolerance and circuit depth increase, these diagnostics will serve as safeguards to ensure that variational quantum algorithms converge towards the correct state, not just a state of low energy.

VI. ACKNOWLEDGEMENTS

I thank Man Hei Cheng for encouragement and helpful discussions regarding this project and the QOLS group for graciously hosting me.

[1] A. Peruzzo, J. McClean, P. Shadbolt, M. Yung, X. Zhou, P.J. Love, A. Aspuru-Guzik, and J. L. O'Brien, "A variational eigenvalue solver on a quantum processor", Nature Communications **5** 4213 (2014), [arXiv:1304.3061v1 [quant-ph]].

[2] K. Bharti, A. Cervera-Lierta, T. H. Kyaw, T. Haug, S. Alperin-Lea, A. Anand, M. Degroote, H. Heimonen, J. S. Kottman, T. Menke, W. Mok, S. Sim, L. Kwek, and A. Aspuru-Guzik, "Noisy intermediate-scale quantum algorithms", Rev. Mod. Phys. **94** 015004 (2022), [arXiv:2101.08448v2 [quant-ph]].

[3] M. Cerezo, A. Arrasmith, R. Babbush, S. C. Benjamin, S. Endo, K. Fujii, J. R. McClean, K. Mitarai, X. Yuan, L. Cincio, and P. J. Coles, "Variational quantum algorithms", Nature Reviews Physics **3** 625 (2021), [arXiv:2012.09265v2 [quant-ph]].

[4] S. Lee, J. Lee, H. Zhai et al, "Evaluating the evidence for exponential quantum advantage in ground-state quantum chemistry", Nature Communications **14** 1952 (2023), [arXiv:2208.02199v3 [physics.chem-ph]].

[5] J. R. McClean, S. Boixo, V. N. Smelyanskiy et al, "Barren plateaus in quantum neural network training landscapes", Nature Communications **9** 4812 (2018).

[6] A. Garcia-Saez and J. I. Latorre, "Addressing hard classical problems with Adiabatically Assisted Variational Quantum Eigensolvers", [arXiv:1806.02287v1 [quant-ph]].

[7] D. Wierichs, C. Gogolin, and M. Kastoryano, "Avoiding local minima in variational quantum eigensolvers with the natural gradient optimizer", Phys. Rev. Res. **2** 043246 (2020), [arXiv:2004.14666v2 [quant-ph]].

[8] T. Haug, K. Bharti, and M. S. Kim, "Capacity and Quantum Geometry of Parametrized Quantum Circuits", PRX Quantum **2** 040309 (2021), [arXiv:2102.01659v2 [quant-ph]].

[9] Z. Holmes, K. Sharma, M. Cerezo, and P. J. Coles, "Connecting Ansatz Expressibility to Gradient Magnitudes and Barren Plateaus", PRX Quantum **3** 010313 (2022), [arXiv:2101.02138v2 [quant-ph]].

[10] M. H. Cheng, K. E. Khosla, C. N. Self, M. Lin, B. X. Li, A. C. Medina, and M. S. Kim, "Clifford circuit initialization for variational quantum algorithms", Phys. Rev. A **111** 062413 (2025), [arXiv:2207.01539v1 [quant-ph]].

[11] P. G. de Gennes, "Collective motion of Hydrogen bonds", Solid State Comm. **1** 6 132137 (1963).

[12] P. Pfeuty, "The one-dimensional Ising model with a transverse field", Annals of Physics **57** 79-90 (1970).

[13] H. Mhiri, R. Puig, S. Lerch, M. S. Rudolph, T. Chotibut, S. Thanasilp, and Z. Holmes, "A unifying account of warm start guarantees for patches of quantum landscapes", [arXiv:2502.07889v1 [quant-ph]].

[14] E. Farhi, J. Goldstone, and S. Gutmann, "A Quantum Approximate Optimization Algorithm", [arXiv:1411.4028v1 [quant-ph]].

[15] D. Wecker, M. B. Hastings, and M. Troyer, "Progress towards practical quantum variational algorithms", Phys. Rev. A **92** 042303 (2015), [arXiv:1507.08969v2 [quant-ph]].

[16] C. H. Bennett, H. J. Bernstein, S. Popescu, and B. Schumacher, "Concentrating partial entanglement by local operations", Phys. Rev. A **53** 2046 (1996).

[17] H. Li and F. D. M. Haldane, "Entanglement Spectrum as a Generalization of Entanglement Entropy: Identification of Topological Order in Non-Abelian Fractional Quantum Hall Effect States", Phys. Rev. Lett. **101** 010504 (2008).

[18] M. A. Nielsen and I. L. Chuang, *Quantum Computation and Quantum Information*, Cambridge University Press (2010).

[19] P. Calabrese and J. Cardy, "Entanglement entropy and quantum field theory", *J. Stat. Mech.* P06002 (2004), [arXiv:hep-th/0405152v3].

[20] L. Xu-Dong Liu and H. Yan, "The Entanglement Entropy of Transverse Field Ising Model", International Journal of Modern Physics and Application **4** 19-23 (2017).

[21] B. Olsthoorn, "Persistent homology of quantum entanglement", Phys. Rev. B **107** 115174 (2023).

[22] F. Igloi and Y. Lin, "Finite-size scaling of the entanglement entropy of the quantum Ising chain with homogeneous, periodically modulated and random couplings", J. Stat. Mech. P06004 (2008).

[23] G. Torlai, K. D. McAlpine, and G. De Chiara, "Schmidt gap in random spin chains", Phys. Rev. B **98** 085153 (2018).

[24] C. Huang, L. Liu, Y. Jiang, and Y. Deng, "Worm-algorithm-type simulation of the quantum transverse-field Ising model", Phys. Rev. B **102** 094101 (2020).

[25] L. Lyu, M. Song, T. Wang, Z. Y. Meng, and W. Witczak-Krempa, "Multiparty entanglement microscopy of quantum Ising models in one, two, and three dimensions", Phys. Rev. B **111** 245108 (2025).

[26] J. Eisert, M. Cramer, and M. B. Plenio, "Colloquium: Area laws for the entanglement entropy", Rev. Mod. Phys. **82** 277 (2010).

[27] K. M. R. Audenaert "A Sharp continuity estimate for the von Neumann Entropy", J. Phys. A **40** 8127–8136 (2007).

[28] R. Wiersema, C. Zhou, Y. de Sereville, J. F. Carrasquilla, Y. B. Kim, and H. Yuen, "Exploring Entanglement and Optimization within the Hamiltonian Variational Ansatz", PRX Quantum **1 020319 (2020)**.